Groundwater dynamics in coastal gravel barriers backed by freshwater lagoons and the potential for saline intrusion: two cases from the UK

Martin J Austin[1,*], Gerd Masselink, Robert T McCall, Timothy G Poate

School of Marine Science and Engineering, Plymouth University, Drake Circus, Plymouth PL4 8AA, UK

Abstract

Field experiments were conducted on two coastal gravel barriers backed by freshwater lagoons to examine the groundwater dynamics and to investigate the potential for saline intrusion. At Slapton Sands, groundwater, lagoon and ocean water level data were collected over a one year period; at Low Bar, data were collected over a two week period. The groundwater table was highly dynamic at both sites, with the ocean tide and wave event signals propagating to within a few metres of the lagoons.

The amplitude and phase lag of the ocean tidal signal as it propagated landwards were used to apply the one-dimensional unsteady groundwater flow equation to estimate the hydraulic conductivity of the barrier aquifers. K is $O(0.01)$ m s^{-1} at both field sites, and this was used with the measured hydraulic gradients to estimate the barrier discharge. Net discharge was directed seawards and strongly positively correlated with the lagoon elevation and large wave events. In contrast, discharge was only weakly correlated with ocean tidal range and lagged by 4 days. This is due to strong landward-directed hydraulic gradients during spring tides reducing the lagoon-derived freshwater flux, with peak discharge occurring mid-way between spring and neap tides. The shoreline of the lagoon was decoupled from the groundwater table at both sites. The groundwater elevation was 1–2 m lower, suggesting that seepage from the lagoon to barrier occurs through the base of the lagoon. This is of potential significance to the modelling of coastal gravel barriers.

Groundwater conductivity measurements demonstrated that salt water penetrates some distance landwards into the barriers (c. 60 m from spring high tide level). However, the width of the barrier systems (120 and 275 m) and the high water level of the fresh water lagoons, c. 0.75–2 m above spring tide level, inhibit saline intrusion.

Keywords: groundwater; gravel barrier; saline intrusion; field experiment; coastal

1. Introduction

Coastal aquifers are complex zones due to the combined influences of oceanic (waves and tides) oscillations and inland groundwater forcing. They are also of significant societal importance for, at least, two main reasons. Firstly, groundwater discharge from coastal aquifers can transport material (e.g. pollutants) from the land to the sea, often at much higher concentrations than in rivers (Windom and Niencheski, 2003). For example, nutrient enrichments of coastal waters has been attributed to groundwater input by a number of researchers and can significantly impact coastal ecosystems (Slomp and Cappellen, 2004; Rao and Charette, 2012). Secondly, saltwater intrusion, which is the ingress of salt water into coastal aquifers, is becoming increasingly widespread and may pose significant problems for agriculture, drinking water supply and fresh water ecosystems (e.g. Andersen et al., 2007). The key factors controlling these two processes are the gradient of the coastal water table and the hydraulic conductivity of the sediment matrix. Significant research efforts

*Corresponding author

Email address: m.austin@bangor.ac.uk (Martin J Austin)

[1]Now at: School of Ocean Sciences, Bangor University, Menai Bridge, Anglesey LL59 5AB, UK

have been expended over the past few decades to better understand and model coastal aquifer dynamics (for a recent overview, refer to special issue of Hydrogeology edited by Post and Abarca (2009)).

In coastal aquifers hydraulically connected to the sea, groundwater levels fluctuate with the rise and fall of the ocean tide, and also respond to offshore wave forcing (Turner and Nielsen, 1997). Typical characteristics of groundwater table fluctuations due to tidal effects include (Nielsen, 1990; Raubenheimer et al., 1999): (1) asymmetric fluctuations with a rapid rise and slow fall; (2) a damped tidal water table fluctuation; and (3) a lag between ocean tidal signal and groundwater table signal. All three characteristics increase in a landward direction. The effect of waves is to pump sea water into the coastal aquifer due to wave runup. This results in a super-elevation of the coastal water table underneath the swash zone and this overheight is directly proportional to the wave height, and also dependent on the beach gradient and wave period (Nielsen, 1990; Masselink and Turner, 2012).

The salinity structure in a tidally-influenced aquifer is also reasonably well-known and consists of a lower saltwater wedge and an upper saline plume (Robinson et al., 2007, 2009; Abarca and Clement, 2009). The saltwater wedge occurs irrespective of wave/tidal action, but the saline plume is due to the tides and results from infiltration in the upper intertidal region, added to by wave action, and exfiltration in the lower intertidal zone. Freshwater exits around the low tide level, and the intense region of mixing between the upper saline plume and the freshwater outflow is known as the sub-terranean estuary (Cooper Jr, 1959; Robinson et al., 2006). Mixing processes in the sub-terranean estuary are considered of great importance to the fate of contaminants and pollutants.

Measurements of the tide-induced groundwater level variations (specifically, the attenuation and time lag of the tidal groundwater signal) can offer important information on the aquifer properties, especially the transmissivity and the hydraulic conductivity (e.g. Erskine, 1991; Trefry and Johnston, 1998; Corbett et al., 2000; Zhou, 2008). The approach generally used for this purpose is the solution to the one-dimensional unsteady groundwater flow model in a confined aquifer, which further assumes that the beach is vertical and that the aquifer is uniform. Strictly speaking this method is only applicable to confined aquifers, but it may also be used for unconfined aquifers if the amplitude of the tidal groundwater table fluctuations are small compared to the depth of an unconfined aquifer and if the observations are made sufficiently far from the intersection between the beach and the groundwater table (Millham and Howes, 1995).

The hydraulic head of the groundwater fluctuates with the tide, but with an amplitude attenuation and phase lag that increase moving landwards from the shoreline. Equation (1) is the standard solution to the one-dimensional unsteady groundwater flow model (e.g. Fetter, 1988; Todd, 1980),

$$H(x,t) = H_0 exp\left(-x\sqrt{\frac{\pi S}{t_0 T}}\right)\sin\left(\frac{2\pi t}{t_0} - x\sqrt{\frac{\pi S}{t_0 T}}\right) \tag{1}$$

where H is the hydraulic head of the aquifer (m), x is distance from the shoreline (m), t is time (d), H_0 is the tidal amplitude (m), t_0 is the tidal period (d), T is transmissivity (m^2 d^{-1}) and S is the specific yield of the aquifer (dimensionless). Fig. 1 defines the aquifers and water levels in the problem coordinate system for a typical coastal gravel barrier cross-section as observed on the southwest coast of the UK.

The amplitude of the water level fluctuations in a cross-shore transect $H(x)$, for example measured using a series of groundwater wells, is related to H_0 by the tidal efficiency factor (TE), described by the first term on the RHS of Equation (1):

$$TE = exp\left(-x\sqrt{\frac{\pi S}{t_0 T}}\right). \tag{2}$$

Equation (2) shows that TE decreases exponentially with distance landwards and the damping constant β is described as:

$$\beta = \sqrt{\frac{\pi S}{t_0 T}}. \tag{3}$$

The temporal lag (t_L) in the arrival of the tidal signal at some distance landward of the shoreline is described by a rearrangement of the second term on the RHS of Equation (1):

$$t_L = x\sqrt{\frac{t_0 S}{4\pi T}}. \tag{4}$$

Equation (4) shows that t_L increases linearly with x, and the slope a is described as:

$$a = \sqrt{\frac{t_0 S}{4\pi T}}. \tag{5}$$

Hydraulic conductivity K is a property of both the porous media and the flowing fluid and is calculated from its relationship with T (Fetter, 1988):

$$T = Kb, \tag{6}$$

where b is the saturated aquifer thickness (m). The solution to Equation (1) via the tidal efficiency or temporal lag is usually referred to as the the tidal damping method. It can be used to determine an integrated estimate for the entire coastal region under consideration (usually a coastal barrier system) and can therefore be more representative than spot measurements of aquifer properties, for example by means of slug tests.

Saline intrusion is the flow of seawater into freshwater coastal areas such as wetlands, lagoons and aquifers, where it can severely disrupt ecosystems (Boulton, 2005) or pollute water supplies (Barlow, 2003). Saline intrusion has typically been observed in regions of groundwater extraction in the coastal zone for potable water, irrigation and industrial uses (Barlow, 2003), but storm surges (Steyer et al., 2007), sea level rise (Feseker, 2007) and water-level fluctuations are increasingly of concern. This is potentially of great significance because many gravel barriers are backed by fresh water lagoon systems, often of high conservation value. In such settings a very pertinent, and in light of anticipated sea-level rise and increased storminess due to climate change increasingly relevant, question relates to the potential for saline intrusion during spring high tides, especially if accompanied by storm surge and energetic wave action.

The rate and pathway of saline intrusion are determined by hydraulic gradients and hydraulic conductivity (Stewart, 1999), so in coastal gravel barrier environments where tidal water level fluctuations may lead to highly dynamic and even reversing hydraulic gradients and where $K \approx 1000$ m day^{-1}, saline intrusion is potentially of great importance. With few exceptions (Erskine, 1991; Austin and Masselink, 2006b; Mao et al., 2006; Turner and Masselink, 2012), the vast majority of research on coastal aquifer dynamics has been conducted along sandy shores with typical values for the hydraulic conductivity K $O(0.0001$ m s^{-1} or 10 m day$^{-1})$. Gravel is much more permeable that sand, with K $O(0.01$ m s^{-1} or 1000 m day$^{-1})$, and a coastal aquifer along a gravel shore is therefore expected to be significantly more responsive to oceanic water table fluctuations (waves, tides, storm surges).

The aim of this paper is to describe and discuss coastal aquifer dynamics across two macro-tidal gravel barrier systems backed by fresh water lagoons. Groundwater level and conductivity measurements were used to determine the necessary properties of the coastal aquifer required to address the potential for saline intrusion. It will be demonstrated that although salt water penetrates into the gravel barriers for a considerable distance, the width of the barrier systems and the relatively high water level of the fresh water lagoons inhibit saline intrusion into the freshwater lagoons.

2. Field methods

2.1. Field sites

Groundwater, tidal and lagoon levels were monitored during 2009–2011 at Slapton Sands, Devon, and during a two-week period in 2012 at Loe Bar, Cornwall, UK (Fig. 2).

2.1.1. *Slapton Sands*

Slapton Sands is a 4-km long gravel barrier with a width of 100–140 m and a crest elevation of 6–7 m above Ordnance Datumn Newlyn (ODN; Fig. 3). The barrier is aligned with a roughly north–south orientation and is backed by a shallow freshwater lagoon (Slapton Ley). The lagoonal water level is approximately 1 m higher than the spring high tide level. The beach has a mean intertidal gradient of $tan\beta = 0.15$ and a median sediment size D_{50} of 6 mm (Austin and Masselink, 2006a). The beach faces east into the English Channel and is consequently sheltered from Atlantic swell. The local wave climate is dominated by periods of southerly and easterly wind-waves. The tidal regime is macro-tidal with spring and neap ranges of 4.3 and 1.8 m, respectively.

2.1.2. *Loe Bar*

Loe Bar is a 1-km long fine-gravel barrier with a maximum width of 250 m and a crest elevation of 9 m ODN (Fig. 3). Loe Bar is aligned roughly east-west and is backed by Loe Pool, a shallow freshwater lagoon. The lagoonal water level is approximately 1.5 m above spring high tide level. The beach has a mean intertidal gradient of $tan\beta = 0.11$ and a median sediment size measured from sediment cores of D_{50} of 2 mm. The beach faces south-west into the English Channel and receives energetic Atlantic swell. The tidal regime is macro-tidal with mean spring and neap ranges of 4.7 and 2.2 m, respectively.

2.1.3. *Water-level control*

The lagoon water levels at both Slapton Sands and Loe Bar are artificially controlled by drainage weirs, which are active during high water levels in order to minimise localised flooding events. At Slapton, van Vlymen (1979) described the lagoon as flow dominated, with a small storage capacity and an unstable water level, which responds rapidly to increased inflow. Therefore through-barrier drainage is not the principal factor in controlling lagoon levels.

2.2. *Boreholes*

At Slapton, five groundwater monitoring boreholes were installed into the barrier by rotary drilling during September 2009. The boreholes penetrate to a depth of approximately -2 m ODN. Each borehole contains a 63 mm diameter polyurethane groundwater well, machine slotted from 0.5 m below ground level to the base. The slotted section of each well is covered by a 250 μm geotextile sock to prevent the ingress of fine sediments. The upper sections of the boreholes are capped with bentonite clay to prevent the vertical ingress of surface water run-off and are topped with a locking steel cover. Similar wells were installed at Loe Bar during March 2012, but these only penetrate to approximately MSL. It is worth noting that, in relation to the size of the barrier, the spatial coverage of the wells at Loe was less than at Slapton Sands.

2.3. *Groundwater monitoring*

2.3.1. *Slapton*

Each groundwater well was equipped with a self-logging LevelTroll absolute pressure transducer, continuously recording pressure and temperature at one-minute intervals; a similar sensor recorded the level of Slapton Ley. A gauge installed on the headland (Matthew's Point) between Slapton and Blackpool Sands sampled the tidal elevation. Barometric pressure was recorded by an additional sensor located in the top-cover of one of the wells; this was reduced to sea-level and used to correct the LevelTrolls for variations in atmospheric pressure. The positions of all sensors were surveyed using an electronic total station and the sensor elevations reduced to ODN. The borehole pressure transducers were downloaded every three months and the tide gauge bi-annually.

A self-recording micro CTD (conductivity, temperature and depth) sensor (INW CT2X) was variously installed into wells BH3–BH5 for periods ranging from 4 to 7 weeks. The CTD was used to measure the groundwater conductivity from which to infer the propagation of salt water into the barrier.

2.3.2. Loe Bar

At Low Bar, each groundwater well was equipped with a self-logging RBR TWR2050 absolute pressure transducer, which recorded pressure and temperature at one-minute intervals. As at Slapton, further sensors were installed into Loe Pool and Porthleven harbour (2-km to the north-west of the field site) to record the lagoon and tidal water levels, respectively. Two INW CT2X CTD sensors were deployed at Loe Bar to measure groundwater conductivity. BH2 was monitored throughout the field experiment, while BH1 and BH3 were each monitored by the CTD sensor for separate 1-week periods.

3. Results

3.1. Water levels

To illustrate the range of water levels observed within the groundwater, lagoon and ocean at Slapton, Fig. 4 plots one year of data recorded by the borehole pressure transducers, tide gauge and wave buoy. Water level variations at four temporal scales can be clearly identified in the groundwater data: (1) a seasonal-scale variation with elevated water levels during winter months; (2) tidal variation at spring-neap and (3) semi-diurnal frequencies; and (4) storm-event scale variations linked to large wave events. The lagoon elevation remains approximately 1 m above the spring high tide elevation and variations in the lagoon water level appear to be at the seasonal and storm-event scales only.

The energy spectrum of the ocean water level fluctuations at Slapton was computed from the average of 16 detrended (to remove seasonal fluctuations) 29-day segments with 50% overlap. The spectrum clearly identified the key tidal constituents and demonstrated the dominance of the semi-diurnal tide (M2,S2) with a period (t_0) of 12.4 hours and the spring-neap variation (14.5 days).

The two-week deployment at Loe Bar reveals groundwater oscillations at the semi-diurnal, spring neap and storm-event timescales; the lagoon level is steady over these timescales (Fig. 5). The lagoon level at Loe Bar is approximately 1 m higher than Slapton Ley and the mean groundwater elevation within the barrier is ∼0.5 m greater. Similarly to Slapton, the Lagoon elevation remains above the spring high tide elevation, in this case by 1.5–2 m.

3.2. Aquifer properties

3.2.1. Slapton

The tidal damping method, Equations (2) and (4), was used to determine TE and t_L for each of the boreholes over 12.4 hour periods resulting in >700 temporal observations. TE was computed as the ratio of the the standard deviation of the water level in the borehole to the standard deviation of the ocean tide level, thereby using all of the data rather than just peak amplitude readings (Erskine, 1991). The temporal lag t_L was computed from the cross-correlation of the water level in each borehole with the ocean tide elevation, and defined as the temporal lag corresponding to the strongest positive cross-correlation peak. The cross-shore distance x for each borehole, was defined as the mean distance from each borehole to the intersection of the ocean tidal elevation with the beach profile for that 12.4 hour period.

The relationship between tidal damping and distance from the shoreline is plotted in Fig. 6. Five large point clouds of TE, each relating to an observation well, display a very weak decay moving landwards away from the shoreline ($x = 0$). The best-fit exponential curve was fitted through the data and suggests that the effect of the ocean tidal variation should be observed at least to the seaward shoreline of the freshwater Ley at $x = 120$ m. Similar point clouds for t_L display a linear increase moving landwards away from the shoreline as suggested by Equation (1) and by e.g. Erskine (1991); Turner et al. (1997).

The slopes of the regression analysis provide the damping coefficient (β = -0.0193 m^{-1}) and slope (a = 1.534 min m^{-1}). Utilising Equations (3) and (5) with $t_0 = 12.41$ hours and $S = 0.25$ (standard value for medium gravel; e.g. Morris and Johnson (1967); Heath (1983)), T is calculated as: $T = 0.4047 \times 10^4$ m^2 d^{-1} (TE); $T = 0.906 \times 10^4$ m^2 d^{-1} (t_L).

Hydraulic conductivity K was calculated using Equation (6), where the mean value for b was determined as 5.6 m from the depth of the clay horizon (-5 m ODN) observed during the borehole drilling and through electrical resistivity measurements at Slapton (Massey et al., 2006). K is estimated as: $K = 0.0084$ m s^{-1}

(TE); K = 0.019 m s^{-1} (t_L). It is encouraging that K determined using both the TE and t_L methods is almost the same order of magnitude, with K_{t_L} approximately twice K_{TE}.

3.2.2. Loe Bar

At Loe Bar, the tidal damping method as employed at Slapton was used over 12.4 hour periods throughout the deployment to provide 24 estimates of TE and t_L. The results are plotted in Fig. 7 and the exponential and linear relationships are fitted to the data; however, the exponential relationship for TE is again very weak.

From the slopes of the regression analysis the damping coefficient is β = -0.0128 m^{-1} and slope a = 0.931 min m^{-1} (Fig. 7). Using the same values for t_0 and S as for Slapton, T is estimated as: T = 0.9293$\times$10^4 m^2 d^{-1} (TE); T = 2.456$\times$10^4 m^2 d^{-1} (t_L). K was calculated using Eq. 6 as K = 0.013 m s^{-1} (TE); K = 0.035 m s^{-1} (t_L), assuming a mean saturated aquifer thickness b of 8 m, determined from the cross-barrier groundwater profiles and borehole sediment cores. Table 1 summarises the measured and inferred aquifer properties for Slapton Sands and Loe Bar. The parameters computed at both sites are very similar with T and K being of the same order of magnitude, $O(10^4)$ m^2 d^{-1} and $O(10^{-2})$ m s^{-1}, respectively.

TABLE 1

3.3. Hydraulic gradients

The rise and fall of the ocean water level at the beachface forces similar variations within the groundwater and establishes time-varying horizontal hydraulic gradients dh/dx (Fig. 8). During spring tides, with typical ranges >4 m, the amplitude of the groundwater variations through the boreholes is ∼1.5 m, whereas during neap tides, when the tide range is ∼2 m, the groundwater amplitude variations are ∼0.5 m; this is roughly in agreement with the predicted linear scaling between tidal and groundwater amplitude in Equation (1). Significant phase lags and amplitude attenuation, which increase in the landward direction, are evident in the groundwater oscillations when compared to the ocean tidal signal and are indicative of tidal damping through the aquifer. Consistent with previous observations (e.g. Emery and Foster, 1948), the groundwater oscillations are also skewed, displaying a faster rise during the flood tide and slower decay during the ebb.

To estimate the local hydraulic gradient, a 2-point method was used, whereby the measured head between adjacent pairs of sensors was differenced and normalised by the cross-shore separation between the pairs.

For the spring tide case (Fig. 8), the ocean tidal elevation begins to exceed the elevation of the groundwater in the boreholes during the mid-flood and a negative dh/dx (landwards-directed) is rapidly established and propagates landwards. $-dh/dx$ is maximum just before high tide (dh/hx = -0.05), before beginning to reduce approximately 2-hours after high water as the ocean tidal elevation decreases and the groundwater elevation increases due to the lagged landward flux of groundwater. The maximum positive (seaward-directed) dh/dx is established around low tide (dh/hx = 0.04), as the falling groundwater levels coincide with the minimum ocean tidal elevation. Across the back-barrier region, dh/dx remains approximately zero or just positive. The negative (landwards-directed) dh/dx during the neap tide case are approximately 30% of those observed for the spring tide and the rate of change over time is also significantly slower; their phasing with respect to the ocean tide is similar.

At Loe Bar, the horizontal hydraulic gradients follow the same trends as at Slapton, but are significantly smaller (Fig. 9). During spring tide conditions, the maximum offshore-directed gradient is $dh/dx = 0.02$, 50 % of that observed at Slapton; the maximum onshore-directed gradient is 20 % of that at Slapton ($-dh/dx =$ 0.01). During neap tides, the offshore-directed gradient is $dh/dx = 0.01$ and the onshore-directed gradients are negligible.

3.4. Barrier discharge

The flow of groundwater through a porous media can be expressed through Darcy's Law (Darcy, 1856) and is given by:

$$Q = -KA\frac{dh}{dx} \tag{7}$$

where Q is the volume of water that flows through cross-section A per unit time, under the local hydraulic gradient dh/dx. The constant of proportionality K is the hydraulic conductivity. Estimating K as 0.01, the

Reynolds number is <10, so Slapton and Loe Bar remain within the acceptable limits for assuming Dacian flow.

The cross-barrier discharge at Slapton was determined by summing Q computed between each pair of wells (excluding the Ley sensor) with equation (7) and then averaging over consecutive 24-hour periods (Fig. 10a). The mean daily discharge was computed as 1.5×10^3 m^3 day^{-1}, per unit barrier width. Comparison with Figure 4 reveals no apparent correlation between Q and the tidal elevation, whereas the large discharge peaks in e.g. November, January and March appear to correlate with peaks in the Ley elevation (h_{Ley}) and H_{rms}. To confirm this observation, the daily time series of Q were cross-correlated against h_{Ley}, H_{rms} and the daily tide range.

Q is strongly positively correlated with h_{Ley} ($r = 0.72$) with a time lag of zero, indicating that peaks in the Ley elevation and discharge are coincident. Q is also positively correlated with H_{rms} ($r = 0.5$) at a time lag of -1-day, suggesting that Q peaks 1 day after large wave events. The smaller value of the correlation coefficient r suggests that the relationship with H_{rms} is weaker then with h_{Ley}. The correlation with the ocean tide range is very low, and hence possibly not significant, but it suggests that daily discharge is negatively correlated with ocean tidal range with greater net discharge occurring 4–5 days after spring tides.

The discharge results for Loe Bar (not shown) are smaller than those measured at Slapton, with a mean discharge of 1.2×10^3 m^3 day^{-1} per unit barrier width. The short length of the time series precludes any meaningful correlation analysis, but the mean discharge is probably representative.

3.5. Aquifer conductivity

At Slapton, groundwater conductivity measurements were made in the three seaward-most boreholes and act as a proxy for salinity (Fig. 11; Table 2). The specific conductivity of the ocean water was measured as 4.23×10^5 μS cm^{-1} and the mean groundwater conductivity decreased rapidly moving landwards towards the Ley, where the specific conductivity was 250 μS cm^{-1}. Two conductivity probe deployments in BH5, for a total of 80 days, show a mean conductivity of 15493 μS cm^{-1} and indicate significant variation with ocean tidal elevation at both the semi-diurnal and spring-neap timescales ($\sigma_C = 9678$ μS cm^{-1}). There is also some indication of variation due to wave forcing (i.e. Jun 2011), where the conductivity variance is increased during neap tide periods. BH4 displays similar amplitude variations in conductivity to BH5, but the mean conductivity is ~40% lower (9537 μS cm^{-1}). Conductivity measured within BH3 is very close to that of the Ley, near-constant (292 μS cm^{-1}) and does not display any significant variation at tidal frequencies ($\sigma_C = 53$ μS cm^{-1}); several small oscillations during late December are probably due to wave forcing. A very short deployment spanning several tidal cycles with the CTD deployed in BH2 (not shown) did not indicate any variation in conductivity.

[TABLE 2]

At Loe Bar, groundwater conductivity was very low and relatively constant over the present temporal and spatial scales (Fig. 12; Table 2). The landward-most well BH1 has a constant conductivity of 291 μS cm^{-1} ($\sigma_C = 11$ μS cm^{-1}), without the semi-diurnal variations in conductivity observed at Slapton. BH2 and BH3, located further seawards, display slightly elevated conductivity (383–462 μS cm^{-1}), but with minimal temporal variation and hence small standard deviations (47–70 μS cm^{-1}). The elevated water levels recorded in BH2–3 towards the end of the deployment period do not lead to increased conductivity. Overall, the conductivity results for Loe Bar suggest that seawater does not significantly propagate into the barrier to the location of the bore holes.

3.6. Lagoon-groundwater shoreline decoupling

At the ocean shoreline the groundwater level is (approximately) coupled to the ocean water level as shown by Equation (1). However, observations made on the back-barrier region at both field sites indicate that this is not the case at the lagoon shoreline. Fig. 13a-b plot the envelopes of groundwater and lagoon water levels and highlight that the groundwater level remains significantly lower than the lagoon level; extrapolating the mean water surface between these points results in unrealistically large hydraulic gradients.

In the region close to the edge of the lagoon, where no boreholes were present, observation pits were excavated to determine the depth of the water table (Fig. 13c). At Loe Bar, this pit was excavated to a depth of 1.9 m before reaching the groundwater, confirming that the barrier water table does not intersect with the lagoon shoreline and is therefore decoupled from the edge of the lagoon. A horizontal tunnel dug from the excavation pit and extending underneath the lagoon bed encountered non-saturated sediments, further confirming that the lagoon level does not represent the terrestrial water table and is in fact perched. The observations at Slapton were similar.

Observations suggest that the bottom of the lagoon is impermeable in the region adjacent to the shoreline and that there is no vertical infiltration of water from the lagoon to the groundwater. Sedimentological analysis indicated that there was no significant difference in grain size distribution between the lagoon bed and barrier matrix. This therefore leaves the question of how the lagoon and barrier groundwater are actually coupled, since Fig. 10 indicates that changes in the lagoon water level are reflected in the barrier groundwater with zero time lag.

4. Discussion

Detailed field measurements of groundwater levels and oceanic forcing conditions collected at two coastal gravel barriers backed by freshwater lagoons within the UK show that the cross-barrier hydraulic gradients are highly dynamic at ocean tide and wave-event timescales. Saline water penetrates a considerable distance landwards, but net seaward-directed hydraulic gradients and high lagoon elevations prevent saline intrusion into the lagoons. In the context of the subterranean estuary (e.g. Robinson et al., 2007), we observe an upper saline plume driven by tide- and wave-induced circulation and a lower lagoon-driven freshwater discharge. It is also observed that the groundwater table is decoupled from the lagoon shoreline, which may have significant implications for the numerical modelling of such environments.

Barrier groundwater levels at both field sites were observed to fluctuate principally at the semi-diurnal tidal frequency with a period of 12.4 hours. Consistent with previous studies on sandy and gravel beaches (Turner et al., 1997; Turner and Masselink, 2012), large wave events also resulted in a super-elevation of the water table across the barrier. The lagoonal water levels remained elevated 1 m and 2 m above the MHWS elevation at Slapton and Loe Bar, respectively. These observations indicate that there must be seaward discharge because there is a substantive hydraulic gradient across the barrier, modulated by the oceanic forcing. To determine the net discharge a Darcian approach was followed whereby the aquifer properties and hydraulic gradients were quantified.

The aquifer properties including the hydraulic conductivity K were computed at Slapton and Loe Bar using the tidal damping method giving $K = O(0.01)$ m s^{-1}. The results were consistent between the two sites using both the tidal efficiency and time lag methods and are comparable to the few previous large scale observations of K. The present estimates are approximately an order of magnitude lower than that obtained by Turner and Masselink (2012) in a prototype-scale laboratory experiment with well-sorted coarse gravel ($D_{50} = 11$ mm) of $K = 0.16$ m s^{-1}. This is consistent with the significantly finer, more poorly sorted gravel and increased proportion of fines in the present field case. It is noteworthy that these values of K are one–two orders of magnitude greater than those along sandy shores where the majority of previous research into coastal aquifer dynamics has occurred.

A common trend throughout both the Slapton and Loe Bar data is the very weak decay in the amplitude of the landwards-propagating ocean tidal signal past the barrier crest. Figures 6 and 7 indicate that there is a significant decay of approximately 60% between the shoreline and the seaward-most borehole, but landwards of that point there is almost no further attenuation of the amplitude signal; however, there is a significant time lag that increases moving landwards. It is thought that this behaviour is due to a departure from one of the simplifying assumptions of the one-dimensional groundwater model: a confined aquifer with a flat base.

The present unconfined aquifer allows variations in transmissivity, which result from fluctuations in the phreatic surface (Erskine, 1991). Combining this with the suggestion from the present data and previous surveys (e.g. Massey et al., 2006) that the aquifer base at Slapton probably slopes upwards moving landwards (due to barrier roll-over), becoming thinner towards the lagoon, it is likely that the groundwater wave shoals moving landwards, minimising the amplitude decay but retaining the phase lag. It is unfortunate that we do not have boreholes located in the rapidly decaying section of the theoretical curves between 0 and 50 m and 0 and 120 m from the shoreline at Slapton and Loe, respectively, which would increase our confidence in the results. However the difficultly of installing wells in such locations is that they would be on the exposed gravel beachface open to wave attack and run-up immersion. Due the above observations, it is preferable to use the time-lag derived aquifer properties; however, the values derived using both the time-lag and tidal-efficiency are very similar.

The measured hydraulic gradients across both barriers are highly dynamic and are principally modulated at the semi-diurnal tidal frequency. Maximum landward-directed gradients of -0.05 (during spring tides at Slapton) are observed across the seaward face of the barrier around high tide as the ocean water level rises across the beachface and these propagate 50 m landwards. The maximum seaward-directed gradients of 0.04 occur at low tide and result from the superposition of oceanic water draining from the beach and the net seepage of terrestrial groundwater/lagoon water. During neap tides, the phasing of the hydraulic gradients is similar, but their magnitude is reduced by approximately 70 % and they only penetrate 40 m landwards. At Loe Bar the net hydraulic gradients are also seaward directed and follow the same trends as at Slapton, but are smaller due to the increased barrier width.

Daily mean values of the net barrier discharge at both Slapton and Loe Bar were always positive and hence seaward-directed. For Slapton, assuming that the barrier is alongshore uniform and homogenous with a wetted gravel length of 3.57 km, multiplying the discharge per unit width by the barrier length provides a mean barrier through flow of 5.4×10^6 m^3 day^{-1}. This is the same order of magnitude as the daily seepage discharge estimated via water balance by van Vlymen (1979). At Loe Bar the daily discharge is 4×10^5 m^3 day^{-1} for a wetted barrier length of 0.32 km.

The net barrier discharge is principally due to the lagoon-driven discharge as indicated by the strong correlation between lagoon-level and daily discharge. During spring tides there is a decrease in net discharge, although the head differences between the groundwater and ocean are maximised, and the hydraulic gradients are large. This is somewhat contrary to the increased discharge observed shortly after large wave events. It is suggested that the ocean tide-induced landward-directed flux during spring tides strongly interacts with the opposing net seaward-directed lagoon discharge, thus reducing the discharge compared to that observed during smaller tide ranges when the landward-directed oceanic flux is smaller. This is demonstrated in Fig. 8, where an increased hydraulic gradient is observed around high tide at the back-barrier indicating a mounding of water at the edge of the lagoon as the inflowing tidal waters hold-up the out-flowing freshwater.

The wave-induced circulation is expected to be conceptually similar to that of the ocean tide, but with significantly smaller volumes of water and at a shallower depth in the aquifer (Cooper Jr, 1959; Robinson et al., 2007). However, unlike for the ocean tidal case, we observe a strong positive correlation between wave events and barrier discharge with a 1-day lag. This is probably due to the wave events blocking up the outflow drain from Slapton Ley. The drain is the principal outflow route from the lagoon weir (e.g. Burt and Heathwaite, 1996) and it flows from a narrow tunnel across the beach at the southern, Torcross, end of the barrier; it is hence vulnerable to being effected by wave-driven morphological change on the beachface. The blockage of the drain is subsequently followed by a rapid increase in the water level of the lagoon, which is observed in Fig. 4 and thus an increase in the net seaward-directed hydraulic gradient and discharge.

Conductivity measurements within the boreholes indicate that there is very limited potential for saline intrusion into the lagoons at Slapton or Loe Bar via the groundwater pathway. At Slapton, significant semi-diurnal variation was observed in the two seaward-most bore holes (BH4-5), but the maximum conductivity measured at BH5 was an order of magnitude less than the seawater and the mean value 2 orders less. The conductivity reduced rapidly moving landwards and by BH3 was consistent with the Ley waters and displayed no semi-diurnal and very minimal wave-induced variability. The measured conductivity across all bore holes at Loe Bar was very low with little spatial or temporal variability. Overall the measured limit of saline intrusion from the mean shoreline at Slapton was 86 m (BH3). At Loe Bar, the landward boundary was a maximum of 129 m (BH3) from the shoreline.

It was observed at both field sites that at the lagoon edge the water table was around 2 m below the ground surface and thus the shoreline of the lagoons were decoupled from the groundwater table. Clearly the lagoons and the groundwater are coupled, since it has been shown that the elevation of the lagoons are of first-order importance in driving subterranean groundwater discharge through the barrier, but this finding suggests that they are coupled at some depth and it is seepage through the base of the lagoon that is important. This is different from observations made in two recent prototype-scale laboratory experiments (BARDEX; Turner and Masselink (2012) and BARDEX II; Masselink et al. (submitted)), where the sediments were well-sorted and the lagoon shoreline remained coupled to the water table. This observation highlights the probable role of fine particles and biological matter that has settled-out across the shallow lagoon periphery and formed a very thin impermeable layer. It also raises an important question for modelling such coastal systems, e.g., how should the barrier-lagoon boundary be treated?

For the numerical modelling of barrier groundwater-ocean dynamics it is clearly insufficient to extrapolate the groundwater table as a continuum between the lagoon and ocean shorelines (e.g. Williams et al., 2012), which will significantly over-estimate the hydraulic gradients across the back-barrier. A simple alternative would be to retain the fixed head assumption, but rather than the fixed head being at the elevation of the lagoon, it should correspond to the expected seepage depth from the lagoon base.

5. Conclusions

Field monitoring campaigns were carried out on two macro-tidal coastal gravel barriers backed by freshwater lagoons to investigate the groundwater dynamics and the potential for saline intrusion. Groundwater and lagoon elevation and conductivity, and oceanic tide and wave forcing were monitored using pressure transducer-logged boreholes and gauges for 1-year at Slapton Sands and 2-weeks and Loe Bar, respectively. It is concluded that:

1. The groundwater levels are highly dynamic across the entire width of the barriers, fluctuating at the semi-diurnal ocean tidal frequency with a period of 12.4 hours. Large ocean wave events during storms result in a super-elevation of the groundwater across the barriers.
2. The ocean tidal signal becomes increasingly lagged and attenuated as it propagates landwards across the barriers. These properties are used to determine the hydraulic conductivity K of the barriers via the one-dimensional unsteady groundwater flow model. K is $O(0.01)$ m s^{-1} at both the Slapton and Loe Bar field sites.
3. The net barrier discharge is principally controlled by the elevation of the lagoons. The lagoons were elevated 1–2 m above the MHWS elevation, thus establishing a seaward-directed hydraulic gradient and hence discharge. At Slapton and Loe Bar the mean daily discharge was 1.5×10^3 and 1.2×10^3 m^3 day^{-1} per unit barrier width, respectively.
4. Barrier discharge peaks around 4 days after the highest spring tides. It is hypothesised that during the peak spring tides, the strong landwards-directed hydraulic gradients reduce the net seaward flux of freshwater. Discharge is also strongly positively correlated to large wave events, but with a lag of 1-day. It is suggested this is due to the blockage of the outflow weir drain from the lagoon, which flows across the beachface, with gravel.
5. The shoreline of the lagoon was observed to be decoupled from the groundwater table at both field sites. The groundwater elevation was 1–2 m lower, suggesting that seepage from the lagoon to barrier groundwater system occurs through the base of the lagoon. This is of potential significance to the modelling of coastal gravel barriers, since extrapolating the groundwater table to the edge of the lagoon will produce unrealistically large hydraulic gradients.
6. The potential for saline intrusion into the freshwater lagoons is low. Groundwater conductivity measurements demonstrated that although salt water penetrates some distance landwards into the barriers (c. 60 m from spring high tide level), the width of the barrier systems (120 and 275 m) and the relatively high water level of the fresh water lagoons (c. 0.75–2 m above spring tide level) inhibit saline intrusion.

Acknowledgements

This project was funded by a Seale-Hayne Educational Trust Grant awarded to MA and GM and an Environmental and Physical Sciences Research Council grant (EP/H040056/1) awarded to GM. We would like to thank the Field Studies Council and the Whitley Wildlife Trust for their assistance at Slapton Sands, and the National Trust for their support at Loe Bar. Tim Scott and Pedro Melo de Almeida are thanked for their field assistance.

References

Abarca, E., Clement, T. P., 2009. A novel approach for characterizing the mixing zone of a saltwater wedge. Geophysical Research Letters 36 (6), 1–5.

Andersen, M. S. G., Baron, L., Gudbjerg, J., Gregersen, J., Chapellier, D., Jakobsen, R., Postma, D., 2007. Discharge of nitrate-containing groundwater into a coastal marine environment. Journal of Hydrology 336 (1-2), 98–114.

Austin, M. J., Masselink, G., 2006a. Observations of morphological change and sediment transport on a steep gravel beach. Marine Geology 229 (1-2), 59–77.

Austin, M. J., Masselink, G., 2006b. Swash – groundwater interaction on a steep gravel beach. Continental Shelf Research 26 (20), 2503–2519.

Barlow, P. M., 2003. Ground water in freshwater-saltwater environments of the Atlantic coast. Tech. Rep. 1262, U.S. Geological Survey.

Boulton, A. J., 2005. Chances and challenges in the conservation of groundwaters and their dependent ecosystems. Aquatic Conservation: Marine and Freshwater Ecosystems 15 (4), 319–323.

Burt, T. P., Heathwaite, A. L., 1996. The hydrology of the Slapton catchments. Field Studies 8, 543–557.

Cooper Jr, H. H., 1959. A hypothesis concerning the dynamic balance of fresh water and salt water in a coastal aquifer. Journal of Geophysical Research 64 (4), 461–467.

Corbett, R. D., Dillon, K., Burnett, W., 2000. Tracing groundwater flow on a barrier island in the North-eastGulf of Mexico. Estuarine, Coastal and Shelf Science 51, 227–242.

Darcy, H., 1856. Dètermination des lois d'ècoulement de l'eau à travers le sable. In: Les fontains Publiques de la Ville de Dijon. Victor Dalmont, pp. 590–594.

Emery, K. O., Foster, J. F., 1948. Water tables in marine beaches. Journal of Marine Research 7, 644–654.

Erskine, A. D., 1991. The Effect of Tidal Fluctuation on a Coastal Aquifer in the UK. Ground Water 29 (4), 556–562.

Feseker, T., 2007. Numerical studies on saltwater intrusion in a coastal aquifer in northwestern Germany. Hydrogeology Journal 15, 267–279.

Fetter, C. W., 1988. Applied Hydrology. Merrill Publishing Company, p. 488.

Heath, R. C., 1983. Basic ground-water hydrology. Water-supply Paper 2220, U.S. Geological Survey.

Mao, X., Enot, P., Barry, D. A., Binley, L. L., Jeng, D. S., 2006. Tidal influence on behaviour of a coastal aquifer adjacent to a low-relief estuary. Journal of Hydrology 327, 110–127.

Masselink, G., Turner, I., 2012. Large-scale laboratory investigation into the effect of varying back-barrier lagoon water levels on gravel beach morphology and swash zone sediment transport. Coastal Engineering 63, 23–38.

Masselink, G., Turner, I. L., Conley, D. C., Ruessink, G., Matias, A., Thompson, C., Castelle, B., Wolters, G., submitted. BARDEX II: Bringing the beach to the laboratory - again! Journal of Coastal Research SI 65, 1–6.

Massey, A. C., Taylor, G. K., Gehrels, W. R., Charman, D. J., 2006. Electrical Resistivity of Coastal Back-Barrier Sediments from South Devon , South-West England , United Kingdom. Journal of Coastal Research 22 (5), 1179–1191.

Millham, N. P., Howes, B. L., 1995. A comparison of methods to determine K in a shallow coastal aquifer. Ground Water 33 (1), 49–57.

Morris, D. A., Johnson, A. I., 1967. Summary of hydrologic and physical properties of rock and soil minerals as analysed by the Hydrologic Laboratory of the U.S. Geological Survey. Water-supply Paper 1839-D, U.S. Geological Survey.

Nielsen, P., 1990. Tidal dynamics of the water table in beaches. Water Resources Research 26 (9), 2127–2134.

Post, V., Abarca, E., 2009. Preface: Saltwater and freshwater interactions in coastal aquifers. Hydrogeology Journal 18 (1), 1–4.

Rao, A. M. F., Charette, M. A., 2012. Benthic nitrogen fixation in an eutrophic estuary affected by groundwater discharge. Journal of Coastal Research 28 (2), 477–485.

Raubenheimer, B., Guza, R. T., Elgar, S., 1999. Tidal water table fluctuations in a sandy ocean beach. Water Resources Research 35 (8), 2313–2320.

Robinson, C., Brovelli, a., Barry, D., Li, L., 2009. Tidal influence on BTEX biodegradation in sandy coastal aquifers. Advances in Water Resources 32 (1), 16–28.

Robinson, C., Gibbes, B., Carey, H., Li, L., 2007. Salt-freshwater dynamics in a subterranean estuary over a spring-neap tidal cycle. Journal of Geophysical Research 112 (C9), 1–15.

Robinson, C., Gibbes, B., Li, L., 2006. Driving mechanisms for groundwater flow and salt transport in a subterranean estuary. Geophysical Research Letters 33 (3), 3–6.

Slomp, C. P., Cappellen, P. V., 2004. Nutrient inputs to the coastal ocean through submarine groundwater discharge: controls and potential impact. Journal of Hydrology 295 (1-4), 64–86.

Stewart, M. T., 1999. Geophysical investigations. In: Bear, J., Cheng, A. H. D., Sorek, S., Ouazar, D., Herrera, I. (Eds.), Seawater Intrusion in Coastal Aquifers - Concepts, Methods and Practices. Kluwer Academic Publishers, pp. 9–50.

Steyer, G. D., Perez, B. C., Piazza, S., Suir, G., 2007. Potential consequences of saltwater intrusion associated with hurricanes katrina and rita. In: Farris, G. S., Smith, G. J., Crane, M. P., Demas, C. R., Robbins, L. L., Lavoie, D. L. (Eds.), Science and the Storms: the USGS Response to the Hurricanes of 2005. U.S. Geological Survey.

Todd, D. K., 1980. Groundwater Hydrology. John Wiley and Sons, Inc, New York.

Trefry, M. G., Johnston, C. D., 1998. Pumping test analysis for a tidally forced aquifer. Ground Water 36 (3), 427–433.

Turner, I. L., Coates, B. P., Acworth, R. I., 1997. Tides, waves and the super-elevation of groundwater at the coast. Journal of Coastal Research 13 (1), 46–60.

Turner, I. L., Masselink, G., 2012. Coastal gravel barrier hydrology — Observations from a prototype-scale laboratory experiment (BARDEX). Coastal Engineering 63, 13–22.

Turner, I. L., Nielsen, P., 1997. Rapid water table fluctuations within the beach face : Implications for swash zone sediment mobility? Coastal Engineering 32 (I 997).

van Vlymen, C. D., 1979. The natural history of Slapton Ley Nature Reserve XIII. the water balance of slapton ley. Field Studies 5, 59–84.

Williams, J. J., Alegría-Arzaburu, A. R. D., Mccall, R. T., Dongeren, A. V., 2012. Modelling gravel barrier profile response to combined waves and tides using XBeach: Laboratory and field results. Coastal Engineering 63, 62–80.

Windom, H., Niencheski, F., 2003. Biogeochemical processes in a freshwater-seawater mixing zone in permeable sediments along the coast of Southern Brazil. Marine Chemistry 83, 121–130.

Zhou, X., 2008. Determination of aquifer parameters based on measurements of tidal effects on a coastal aquifer near Beihai, China. Hydrological Processes 22, 3176–3180.

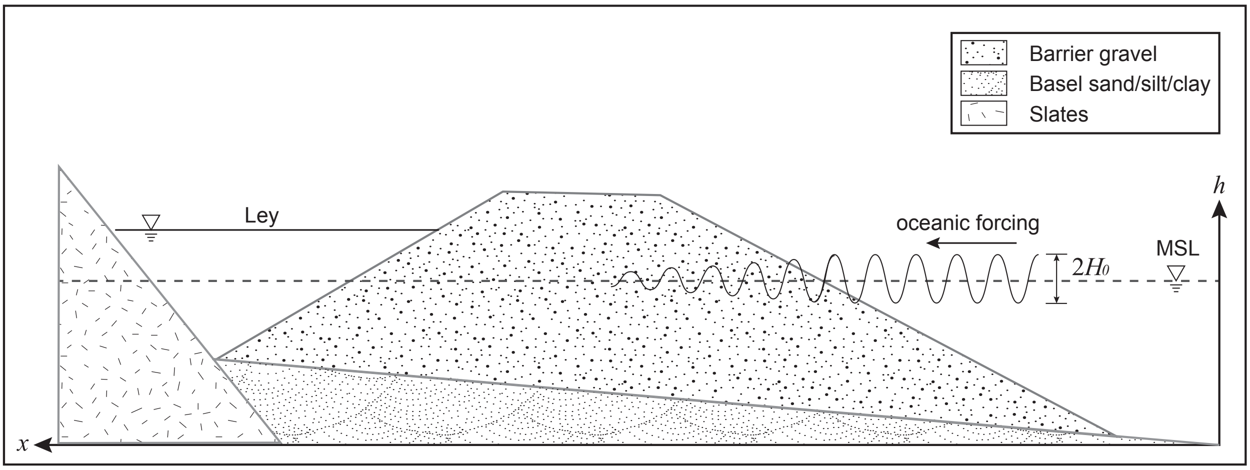

Figure 1: Conceptual diagram of a barrier cross-section indicating the aquifer arrangement and water levels in the problem co-ordinate system.

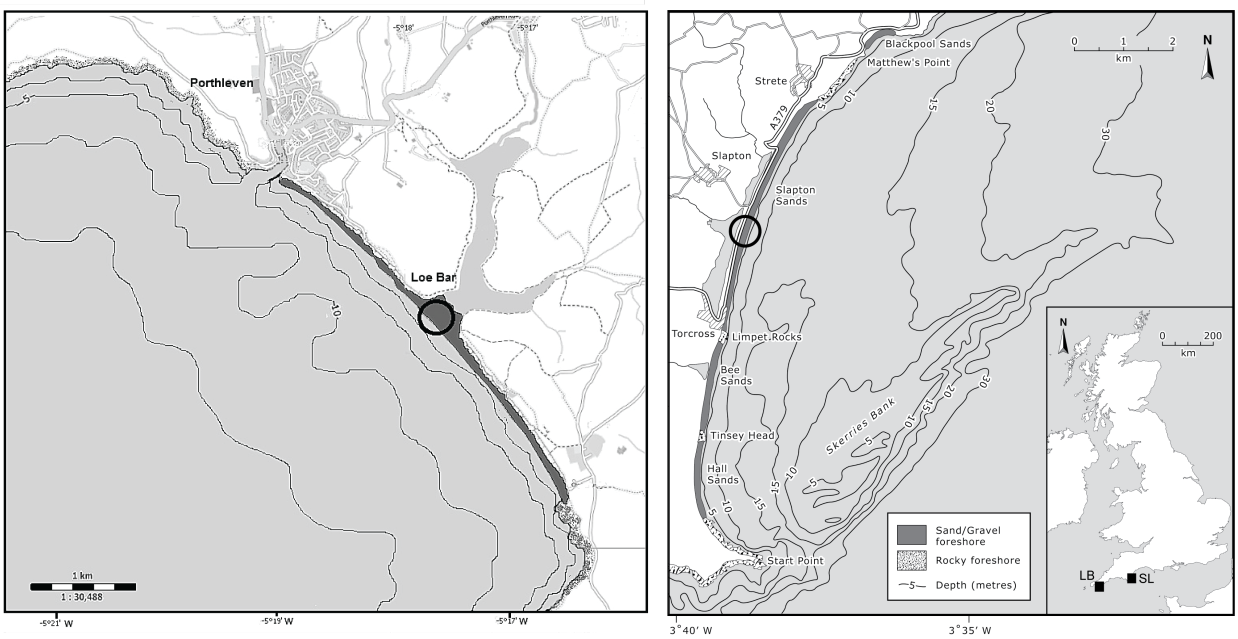

Figure 2: Location maps of (left) Loe Bar and (right) Slapton Sands. The field sites are marked by the squares in the inset map.

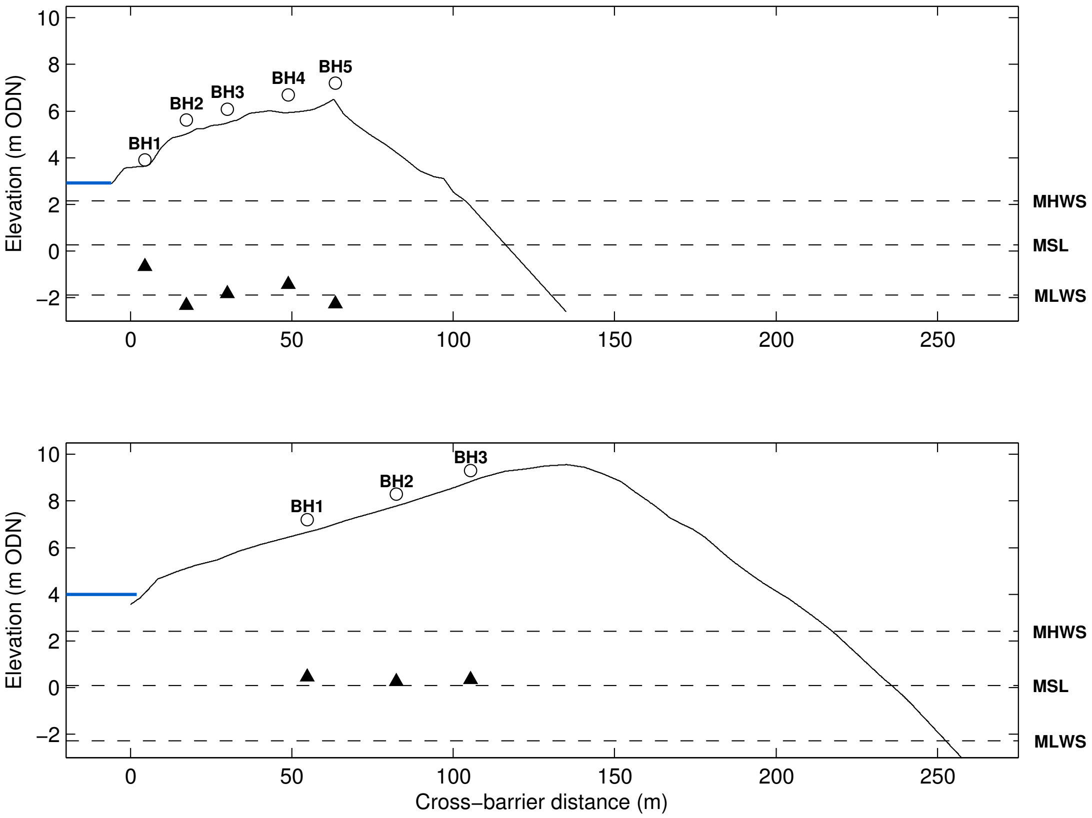

Figure 3: Cross-barrier profile of Slapton Sands (top) and Loe Bar (bottom) indicating borehole locations (circles) and pressure transducers (triangles). The mean lagoon elevation is shown by the heavy blue line. Mean sea level (MSL), mean high water spring (MHWS) and mean low water spring (MLWS) level are shown by the horizontal dashed lines.

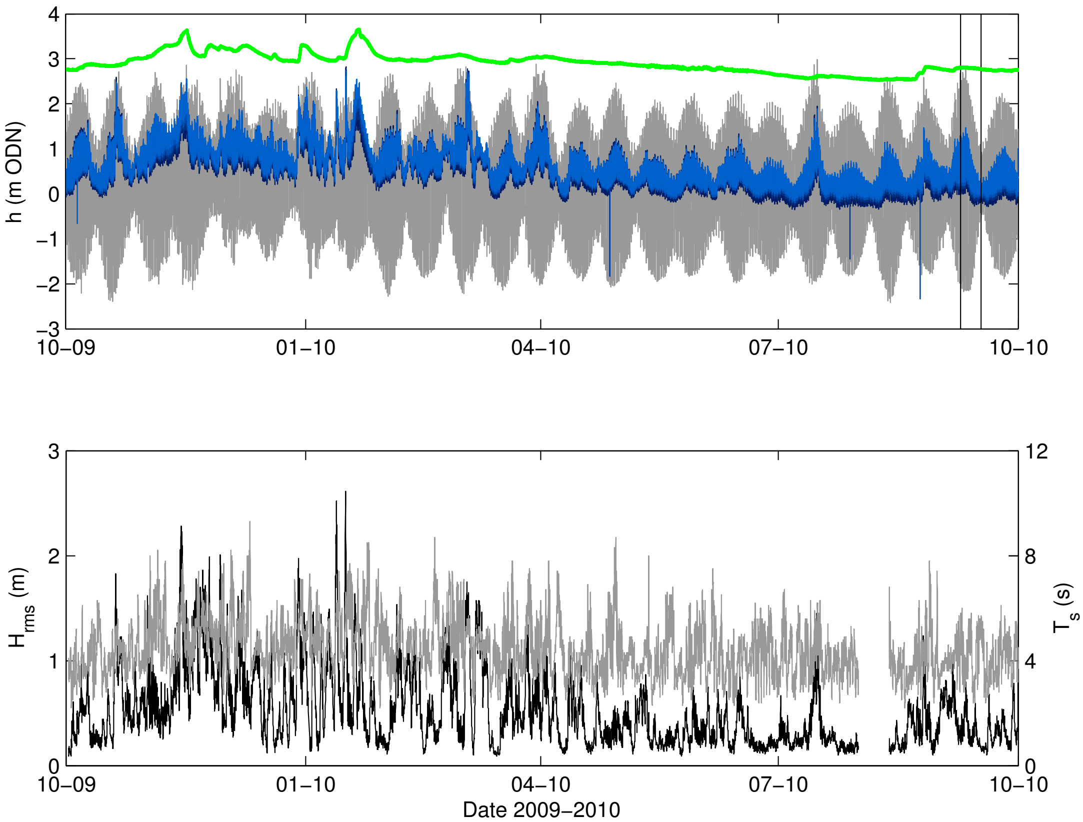

Figure 4: Overview time series of water level data from Slapton. (Top) Water levels recorded in the boreholes (blue), Ley (green) and tide (grey). (Bottom) Root mean square wave height H_{rms} (black, left axis) and significant wave period T_s (grey, right axis) recorded by the wave buoy. The two vertical black lines in September in the upper panel identify the spring and neap cycles discussed in Fig. 8.

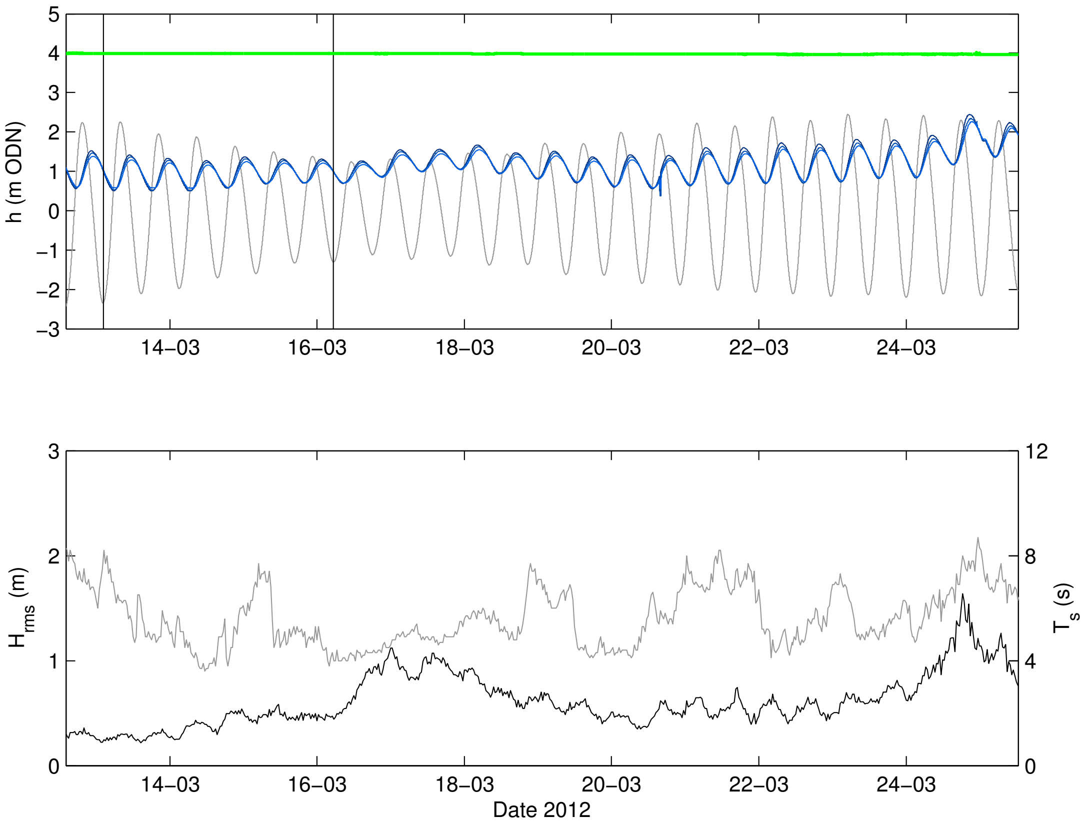

Figure 5: Overview time series of water level data from Loe Bar. (Top) Water levels recorded in the boreholes (blue), lagoon (green) and tide (grey). (Bottom) Root mean square wave height H_{rms} (black) and significant wave period T_s (grey) recorded by the wave buoy. The two vertical black lines in the upper panel identify the spring and neap cycles discussed in Fig. 9

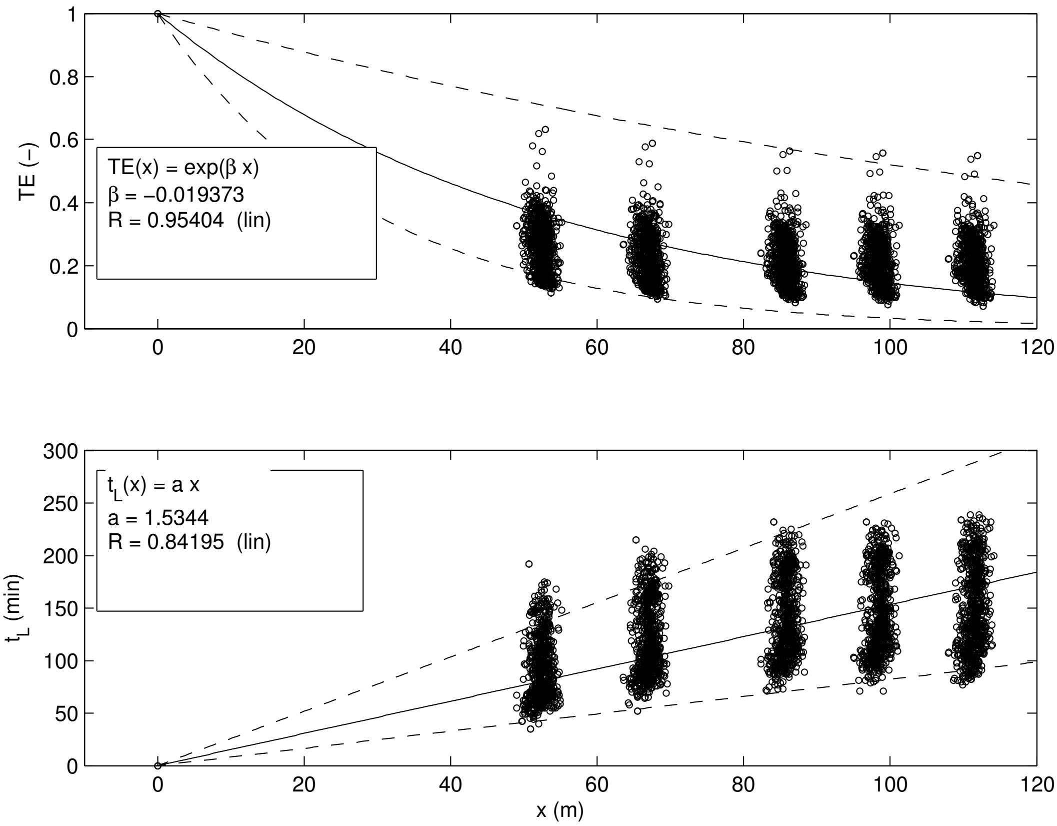

Figure 6: Slapton: Tidal efficiency factor TE (top) and time lag t_L (bottom) plotted against distance from the shoreline. TE and t_L were computed for each 12.5 hour tidal cycle. The solid lines plot the exponential and linear best-fit lines for the TE and t_L, respectively and the dashed lines display the envelope of the best-fit.

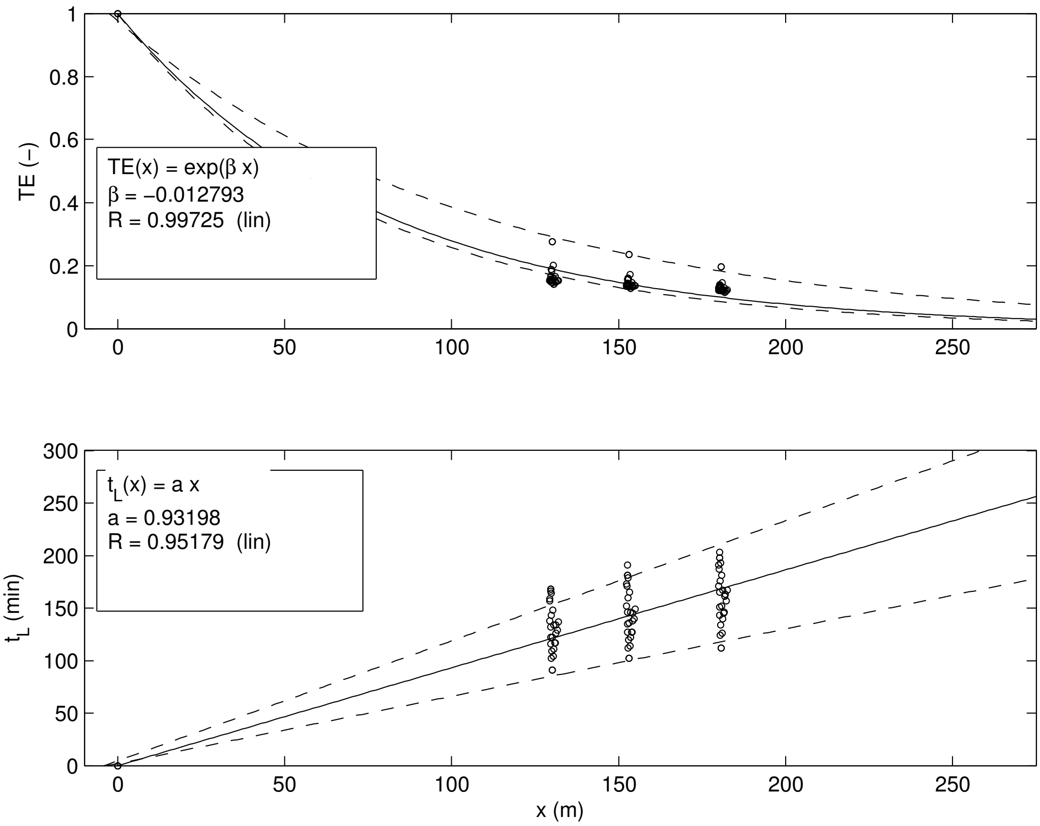

Figure 7: Loe Bar: Tidal efficiency factor TE (top) and time lag t_L (bottom) plotted against distance from the shoreline. TE and t_L were computed for each 12.5 hour tidal cycle. The solid lines plot the exponential and linear best-fit lines for the TE and t_L, respectively and the dashed lines display the envelope of the best-fit.

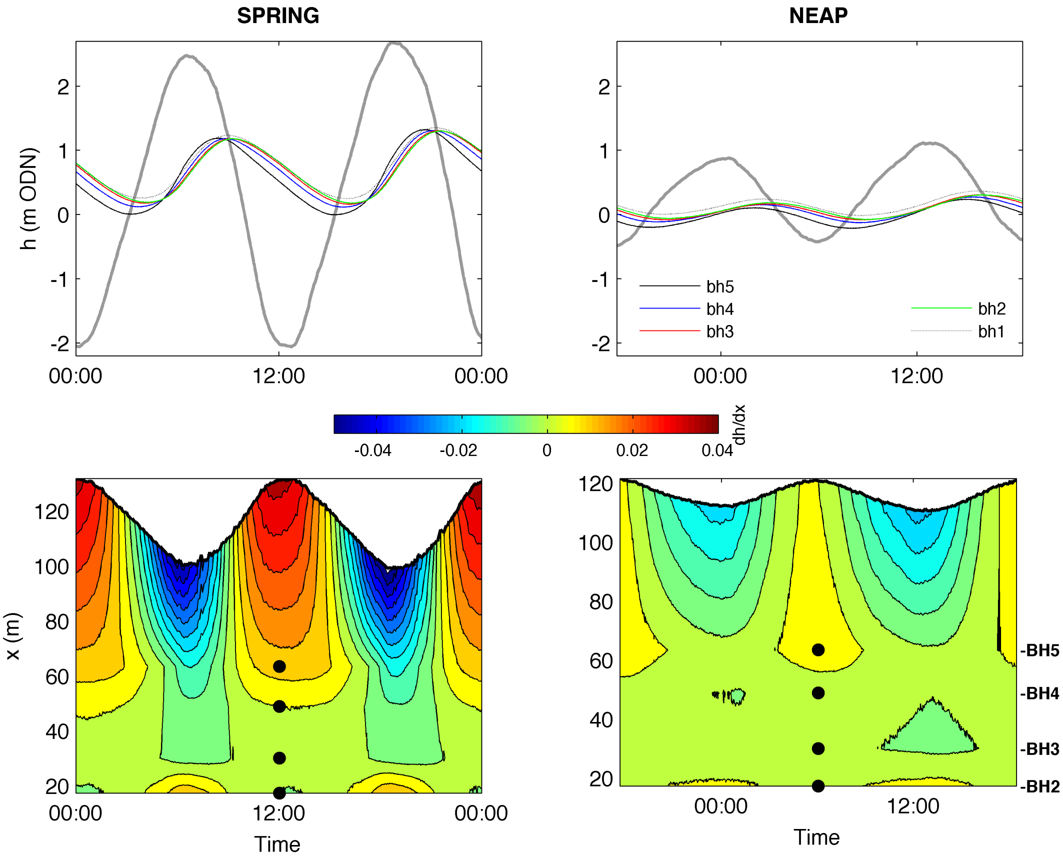

Figure 8: Groundwater level variations and hydraulic gradients at Slapton during the spring (left) and neap (right) tides highlighted in Fig. 4. (Top) Tidal water level (grey line) and groundwater elevation at each of the five boreholes. (Bottom) Contours of hydraulic gradient dh/dx (positive seawards), where the solid black markers indicate the cross-shore location of the boreholes and the thick black line the movement of the ocean shoreline.

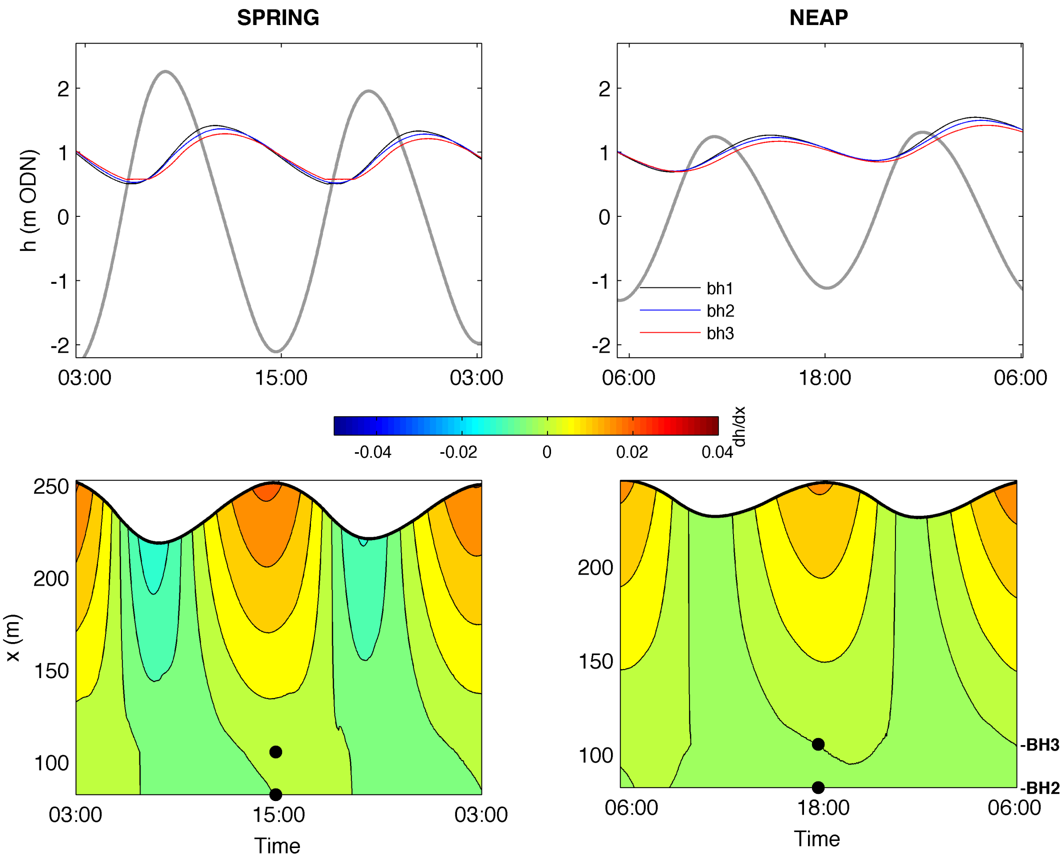

Figure 9: Groundwater level variations and hydraulic gradients at Loe Bar during the spring (left) and neap (right) tides highlighted in Fig. 5. (Top) Tidal water level (grey line) and groundwater elevation at each of the five boreholes. (Bottom) Contours of hydraulic gradient dh/dx (positive seawards).

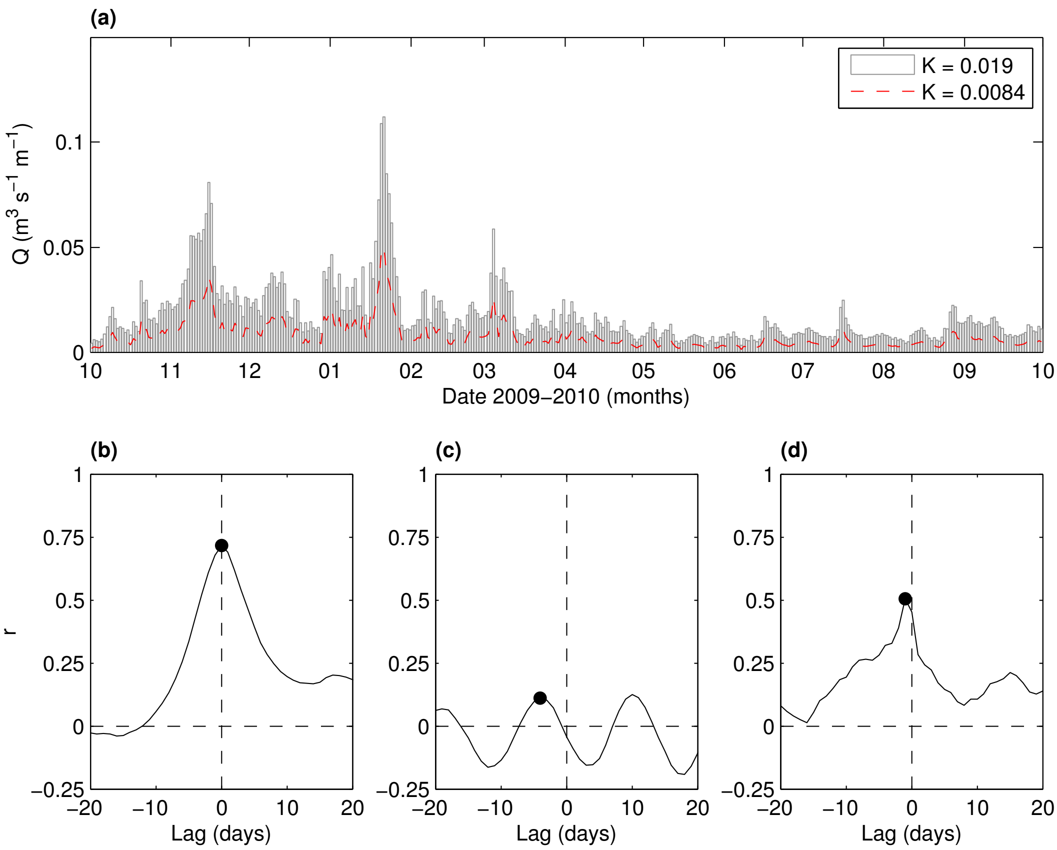

Figure 10: Slapton groundwater discharge Q. (a) Daily-averaged groundwater discharge per unit barrier width for the two computed values of K, positive seawards; cross-correlation of daily-averages of (b) Q and the Ley elevation; (c) Q and the tidal range; and (d) Q and H_{rms}. Solid dots indicate the time lag at the maximum positive correlation.

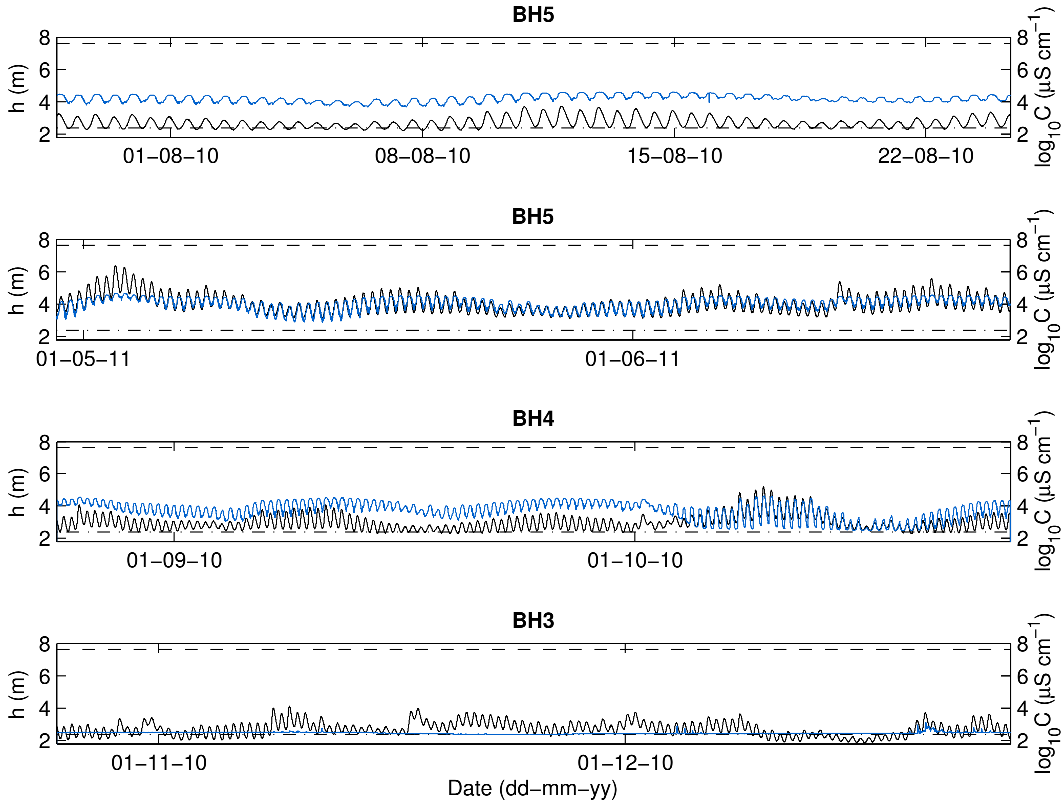

Figure 11: Time series of groundwater conductivity (blue lines, right axis, log-scale) and groundwater level (black lines, left axis) measured in boreholes BH3–BH5. The horizontal dashed black line indicates the measured log-scale seawater conductivity and the dot-dash line the Ley conductivity. Note that the time periods are not coincident.

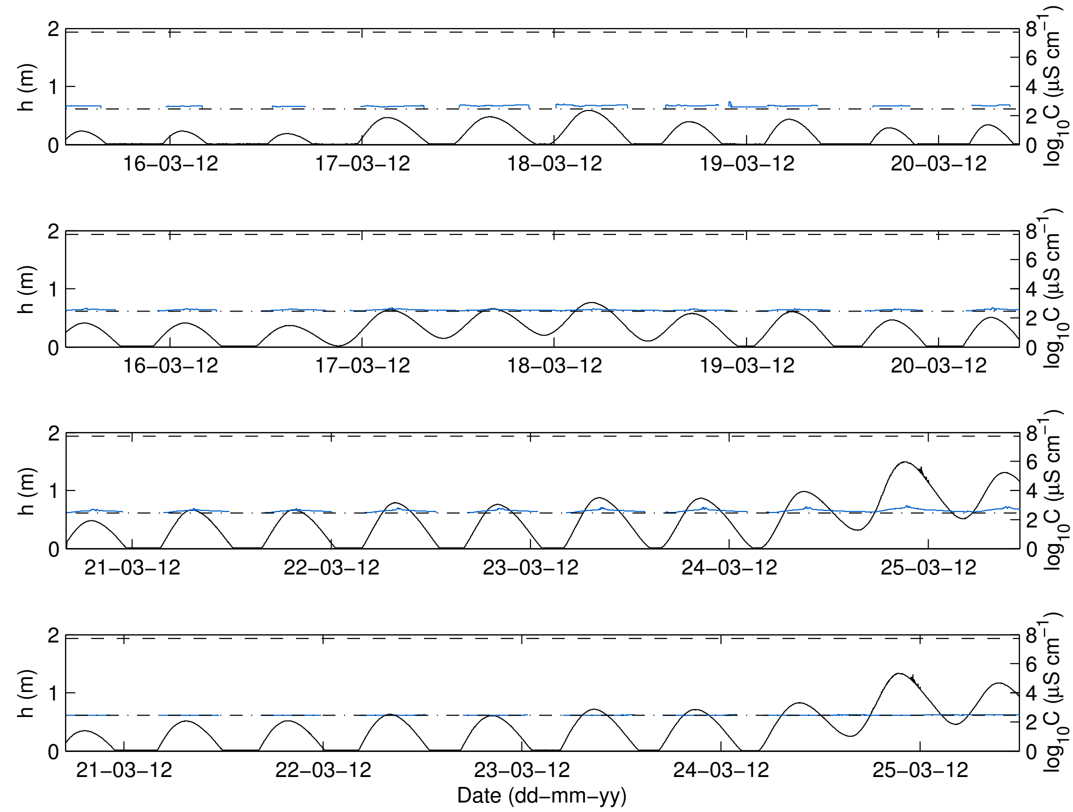

Figure 12: Time series of groundwater conductivity (blue lines, right axis, log-scale) and groundwater level (black lines, left axis) measured in boreholes BH1–BH3. The horizontal dashed black line indicates the measured log-scale seawater conductivity and the dot-dash line the lagoon conductivity. Note that the time periods for panels 1 and 2, and 3 and 4, respectively, are coincident. The gaps in the conductivity record are due to the sensor drying out.

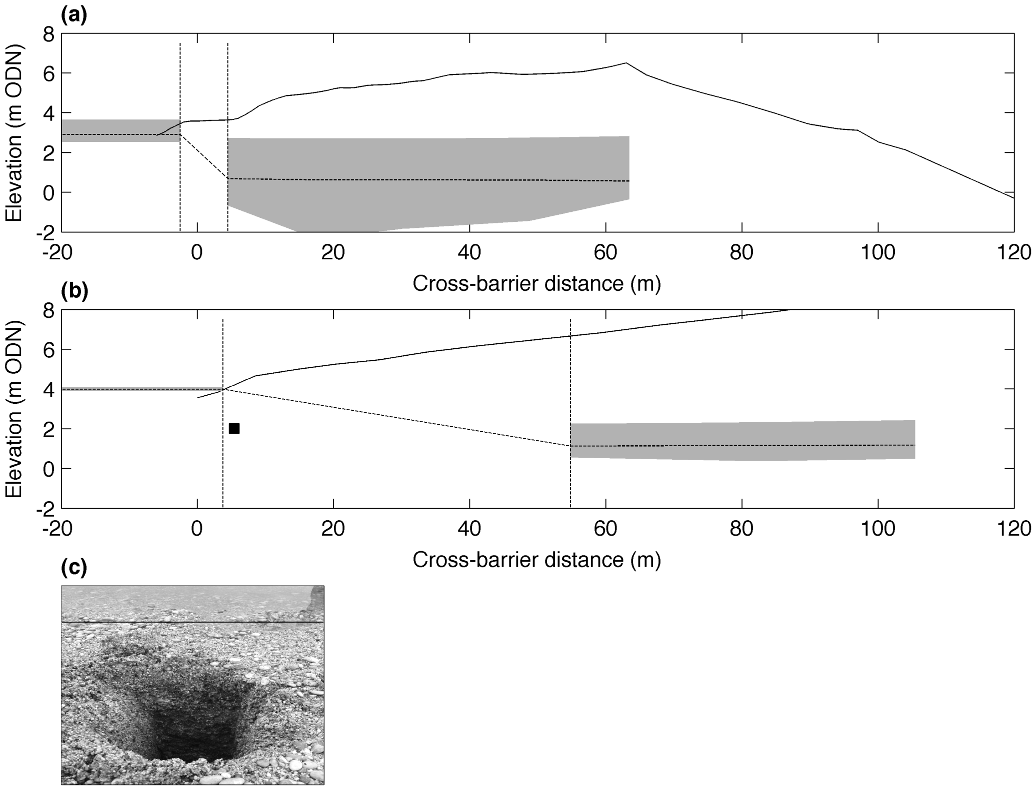

Figure 13: Lagoon-groundwater decoupling. Cross-barrier profiles indicating the envelope of groundwater and lagoon water levels (grey shading) for (a) Slapton and (b) Loe Bar. The vertical dashed lines indicate the region at the lagoon edge with no direct groundwater level measurements. The horizontal dashed lines show the mean groundwater profile (inferred between the vertical dashes). (c) Photograph of the observation pit excavated close to the lagoon at Loe Bar. The solid line highlights the lagoon shoreline. The solid square in (b) plots the location of the base of the observation pit.

Table 1: Summary of the aquifer properties inferred from measurements at Slapton Sands and Low Bar. TE is the tidal efficiency method and t_L is the tidal lag method.

	Slapton Sands		Loe Bar	
	TE	t_L	TE	t_L
a (min m^{-1})	-	1.5344	-	0.931
β (m^{-1})	-0.0193	-	-0.0128	
T (m^2 d^{-1})	0.4047×10^4	0.906×10^4	0.9293×10^4	2.456×10^4
S (-)	0.25	0.25	0.25	0.25
b (m)	5.6	5.6	8	8
K (m s^{-1})	0.0084	0.019	0.013	0.035

Table 2: Overview of measured groundwater conductivity in the boreholes. x is the distance landwards from the mean shoreline position. Note: measured seawater conductivity at Slapton = 4.23×10^5 μS cm^{-1}.

	$\overline{C}$	σ_C	min(C)	max(C)	x
	(μS cm^{-1})	(μS cm^{-1})	(μS cm^{-1})	(μS cm^{-1})	(m)
Slapton					
BH5	15493.32	9678.20	753.20	46510.90	53
BH4	9536.47	8712.81	309.10	42534.00	68
BH3	291.96	53.42	241.50	1317.70	86
Loe Bar					
BH3	462.27	47.85	253.60	878.10	129
BH2	383.72	70.09	251.10	918.90	152
BH1	291.04	11.00	257.50	336.70	180